Electronic Supplementary Material (ESI) for Journal of Materials Chemistry C.

Supporting Information

Ultrasensitive Turn-on Luminescence Humidity Sensor Based on a Perovskite/Zeolite Composite

Yu-Jie Gao,[a] Giacomo Romolini,[b] Haowei Huang,[a] Handong Jin,[b] Rafikul Ali Saha,[a] Biplab Ghosh,[a] Michiel De Ras,[b] Chunhua Wang,[b] Julian A. Steele,[a,c] Elke Debroye,[b] Johan Hofkens[b] and Maarten B. J. Roeffaers*[a]

[a] Department of Microbial and Molecular Systems, Centre for Membrane Separations, Adsorption, Catalysis and Spectroscopy for Sustainable Solutions (cMACS), KU Leuven, Celestijnenlaan 200F, 3001 Leuven, Belgium.

[b] Department of Chemistry, Faculty of Sciences, KU Leuven, Celestijnenlaan 200F, 3001 Leuven, Belgium.

[c] School of Mathematics and Physics, The University of Queensland, Brisbane, QLD, 4072, Australia.

† E-mail: maarten.roeffaers@kuleuven.be

Experimental section.

Materials and Chemicals. Na^+-FAU-Y zeolite (CBV 100, Si/Al = 2.55, Zeolyst), cesium bromide (CsBr, Sigma-Aldrich, 99.9%), lead bromide ($PbBr_2$, Sigma-Aldrich, ≥ 98%), 1-octadecene (J&K Scientific, 90%), oleic acid (OAc, Sigma-Aldrich, 90%), oleylamine (OAm, Sigma-Aldrich, 70%) and hexane (Chem-Lab, ≥ 98%) were used without further purification.

Preparation of Cs^+/Na^+-FAU-Y: A mixture of 1.0 g FAU-Y and 200 mL 0.25 M CsBr aqueous solution was shaken in an end-over-end shaker at 80 °C for 16 h. The product was centrifuged and washed with deionized water 3 times. Then it was dried at 80 °C under vacuum for 24 h.

Preparation of $PbBr_2$ Solution: $PbBr_2$ (70.5 mg), ODE (2.5 mL), OAc (0.5 mL), and OAm (0.5 mL) were mixed and dried under N_2 flow at 120 °C. After the $PbBr_2$ was completely dissolved, the solution was allowed to cool down to room temperature under the N_2 atmosphere.

Synthesis of Cs_4PbBr_6/FAU-Y: A mixture of Cs^+/Na^+-FAU-Y (250 mg) and ODE (3 mL) was loaded in a 25 mL three-neck flask, kept stirring, and dried under N_2 flow for 1 h at 120 °C. Then the temperature was raised to 150 °C under N_2 atmosphere and the $PbBr_2$ solution was injected. The mixture was stirred for 15 min and then cooled down by an ice-water bath. Finally, the product was washed with dry hexane 3 times and dried at 60 °C under vacuum for 12 h.

Synthesis of Cs_4PbBr_6 NPs and Cs_4PbBr_6/SiO_2: The synthesis of Cs_4PbBr_6 NPs was performed according to a published method.[1] Cs_2CO_3 (0.16 g, 0.49 mmol) , 16 mL ODE and 1 mL OAc was added into 50 mL three-neck flask, kept stirring, dried for 1 h at 120 °C under vacuum. Then the mixture was heated under N_2 to 150 °C until all Cs_2CO_3 reacted with OAc to form cesium-oleate solution. In a typical synthesis of Cs_4PbBr_6 NPs, $PbBr_2$ (0.2mmol), OAm (1 mL), OAc (1 mL,), and ODE (10 mL) and were loaded into 50 mL three-neck flask and dried under vacuum for 1 h. The reaction mixture was heated to 140 °C. Then, 10 mL hot (~150 °C) Cs-oleate solution was rapidly injected into the $PbBr_2$ solution. After 10 s , the reaction mixture was immediately cooled bysubmerging the flask in an ice-water bath. The nanoparticles were extracted from the crude solution by centrifuging at 7000 rpm for 5 min. After that, the supernatant was removed and the precipitate was re-dispersed in dry hexane, then centrifuged at 3000 rpm for 5 min to get high-quality nanoparticles. To synthesize Cs_4PbBr_6/SiO_2, nonoporous SiO_2 were added into the $PbBr_2$ solustion. Other steps of Cs_4PbBr_6 NPs synthesis are as same as pure Cs_4PbBr_6 NPs synthesis.

Synthesis of Cs_4PbBr_6 LPs: The synthesis of Cs_4PbBr_6 LPs was based on a previously reported method.[2] In summary: CsBr (0.8 mmol; 0.1697 g) and $PbBr_2$ (0.2 mmol, 0.1468 g) were dissolved in 6mL a 50:50 (v:v)mixture of 3 mL DMF and 3 mL DMSO. 0.25 mL OAc and 0.25 mL OAm were added to stabilize the precursor solution. The, 6 mL precursor solution was rapidly injected into 50 mL toluene under vigorous stirring for 1 min. The suspension was immediately centrifuged at 6000 r/ min for 5 min and the precipitate was collected.

Physical Measurements. Scanning electron microscope (SEM) analyses were performed with an FEI-QFEG250 system. Transmission electron microscopy (TEM) images of samples were obtained using a probe-lens corrected JEOL ARM200F operating at 200 kV, equipped with cold-field emission source and Centurion EDX detector. X-ray diffraction (XRD) patterns were meausred in a Malvern PANalytical Empyrean diffractometer in reflection or transmission mode, where in the latter case the sample was loaded in a glass capillary with a diameter of 0.5 mm and kept under spinning for the whole duration of the measurement. The diffractometer is equipped with PIXcel3D solid-state detector and a Cu anode $K\alpha$, and the powder

diffraction was measured in the angular range of 2Θ= 2-45° at room temperature. The XRD data were analyzed using the Rietveld technique and Le-Bail refinements were done using the FULLPROF program.[3] The steady-state photoluminescence was recorded on an Edinburgh FLS980. The optical absorption spectra of the samples were obtained on a Lambda-950 UV-vis spectrometer. X-ray photoelectron spectroscopy (XPS) was carried out on an ESCALAB 250Xi X-ray Photoelectron Spectrometer. XPS data have been fitted using KolXPD software. For the fitting Shirley background has been considered. For the peak fitting spin-orbit doublet has been used, which consists of two convolutions of a Lorentzian and a Gaussian peak, represented by 2L*G. Atomic absorption spectroscopy (AAS) was performed with a ContrAA 700.

Humidity testing of Cs_4PbBr_6/FAU-Y. The humidity sensing characterizations were performed by exposing the sensor Cs_4PbBr_6/FAU-Y to atmospheres with a different relative humidity (RH). Moisture conditions of various RH values were achieved by using different saturated salt solutions according to previous literature.[4] Saturated salt solutions of LiBr, $CaI_2{\cdot}6H_2O$, $CaAc_2{\cdot}H_2O$ and sucrose, $CaAc_2{\cdot}H_2O$, $MgCl_2$, K_2CO_3, NaBr, KI, KCl, and K_2SO_4 at 25 °C were equilibrated in closed wide-mouth bottles for 12 h to provide different constant RH values of 7%, 11%, 13%, 17%, 33%, 45%, 59%, 70%, 85% and 98% respectively.

Table S1 The results of AAS characterization for pristine FAU-Y, Cs^+/Na^+-FAU-Y, and Cs_4PbBr_6/FAU-Y.

	Na (wt. %)	Cs (wt. %)	Pb (wt. %)
Pristine FAU-Y	6.32	0	0
Cs^+/Na^+-FAU-Y	2.02	57.13	0
Cs_4PbBr_6/FAU-Y	1.69	38.42	9.22

To calculate the Cs^+/Na^+ exchange efficiency, we assumed the weight of the material to be 1 g. Therefore, in 1 g of pristine FAU-Y, the weight of Na^+ is 63.2 mg corresponding to 2.74 mmol. After the Cs^+/Na^+ exchange, the moles of Na and Cs are 0.879 mmol and 4.29 mmol, respectively. Then, the Cs^+/Na^+ exchange efficiency can be calculated from the following equation:

$$Cs/Na\ exchange\ efficiency = \frac{Moles\ of\ Na\ before\ exchange - Moles\ of\ Na\ after\ exchange}{Moles\ of\ Na\ before\ exchange} \times 100\% = \frac{2.74 - 0.879}{2.74} \times 100\% = 67.9\%$$

The Cs^+/Na^+ exchange efficiency, 67.9%, is in the range of the maximum value of the conventional method (66%–69%).[5] Thus, 1.86 mmol Cs^+ exchanged the Na^+ to enter the framework of FAU-Y and the other 2.43 mmol Cs^+ adsorbed on the surface of FAU-Y.

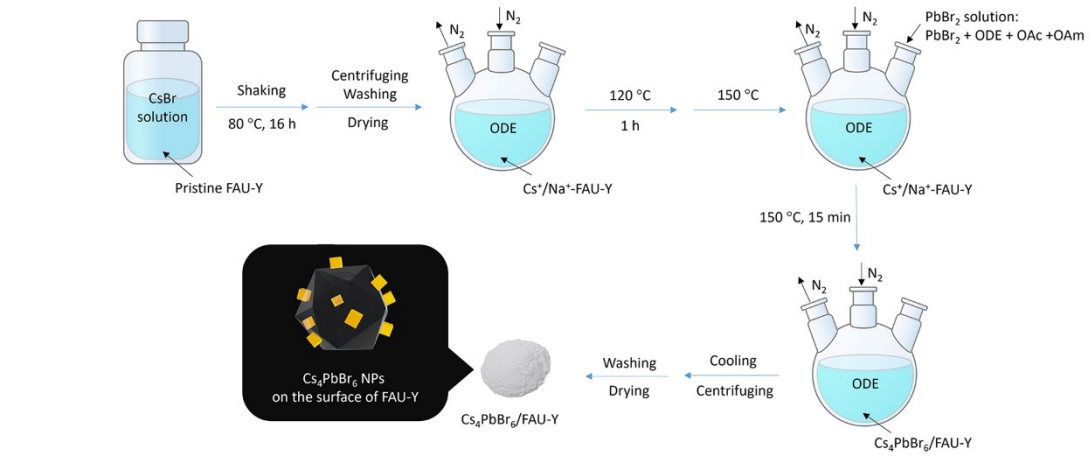

Figure S1 Scheme showing the synthesis procedure of the perovskite/zeolite composite (Cs_4PbBr_6/FAU-Y).

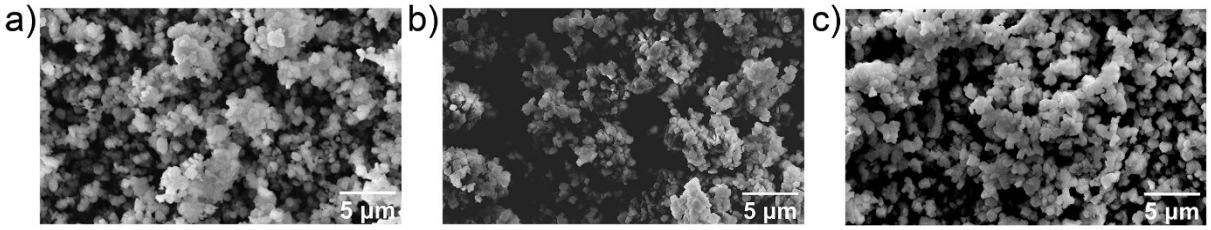

Figure S2 SEM images of (a) pristine FAU-Y, (b) Cs^+/Na^+-FAU-Y, and (c) Cs_4PbBr_6/FAU-Y.

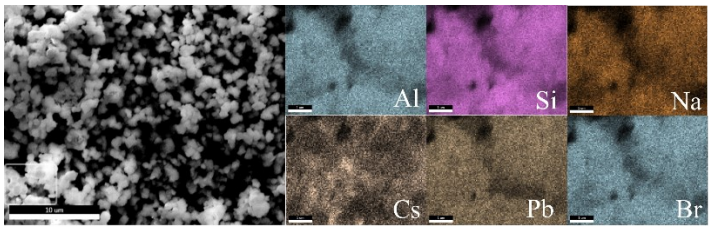

Figure S3 Elemental distribution mapping of Cs_4PbBr_6/FAU-Y.

As shown in Fig. S2, the SEM images of pristine FAU-Y, Cs^+/Na^+-FAU-Y, and Cs_4PbBr_6/FAU-Y reveal no obvious morphological difference between the samples. Elemental mapping of the Cs_4PbBr_6/FAU-Y exhibited the presence of a significant amount of Cs, Pb, and Br, which are uniformly distributed on the FAU-Y (Fig. S3).

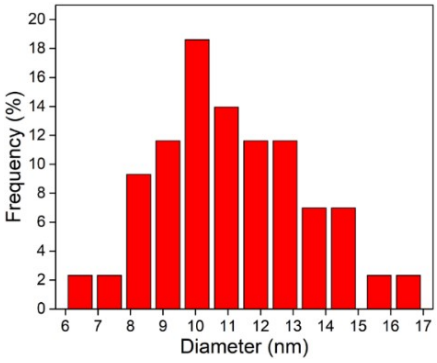

Figure S4 The particle size distribution of perovskite particles anchored on the surface of FAU-Y.

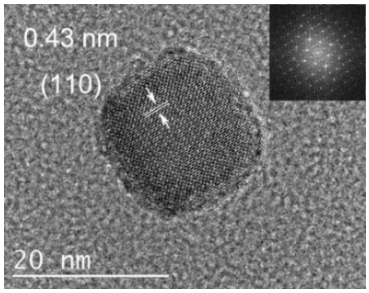

Figure S5 HRTEM image of Cs_4PbBr_6/FAU-Y composite, which was wetted with trace water (10 mg composite were added 2 μL water). The inset is the electron diffraction diagrams of the formed $CsPbBr_3$ particle.

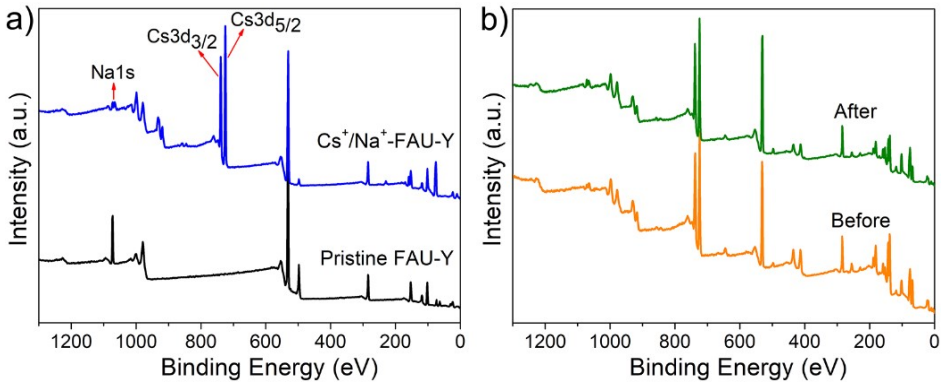

Figure S6 The survey XPS spectra of (a) pristine FAU-Y and Cs^+/Na^+-FAU-Y, (b) Cs_4PbBr_6/FAU-Y before and after exposure to air.

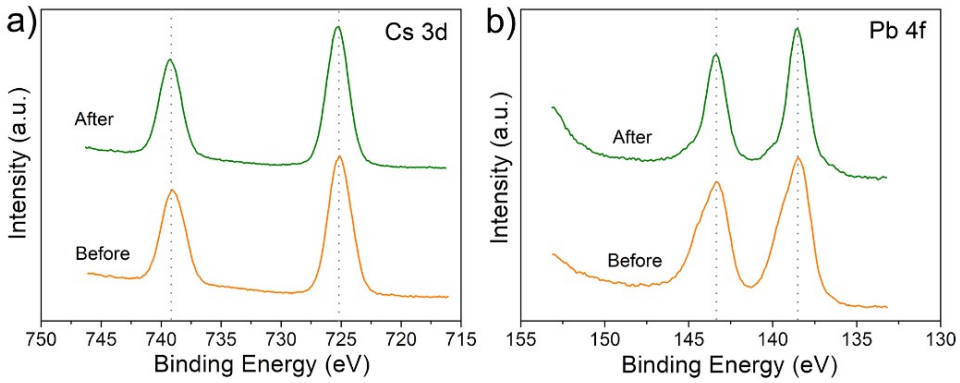

Figure S7 (a) Cs 3d and (b) Pb 4f XPS spectra of Cs_4PbBr_6/FAU-Y before and after exposure to air.

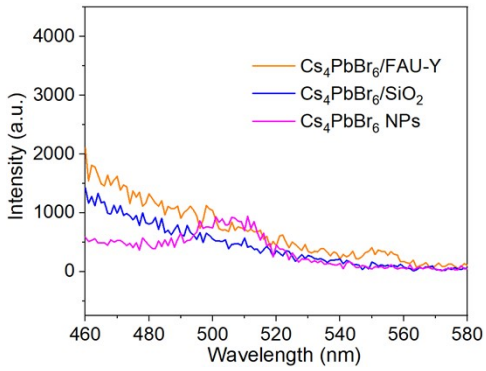

Figure S8 The emission spectra of Cs_4PbBr_6/FAU-Y, Cs_4PbBr_6 NPs, and Cs_4PbBr_6/SiO_2 before exposure to moisture, which were dispersed in the hexane solution.

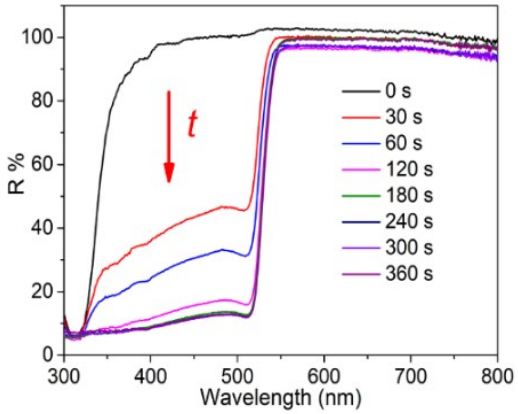

Figure S9 UV-Vis diffuse reflectance spectra of Cs_4PbBr_6/FAU-Y composite after exposure to 45% RH for different times.

UV-Vis diffuse reflectance spectra were recorded after exposing Cs_4PbBr_6/FAU-Y composite to 45% RH at different times, which reflects the time-dependent structural transformation from Cs_4PbBr_6 to $CsPbBr_3$ (Fig. S9). After exposure at RH of 45%, a new absorption band at around 510 nm, which belongs to $CsPbBr_3$, appeared and fast became stronger. Meanwhile, the absorption band of Cs_4PbBr_6 at 315 nm decreased. It is worth noting that almost all Cs_4PbBr_6 of the composite transformed to $CsPbBr_3$ after exposure with an RH of 45% for 180 s.

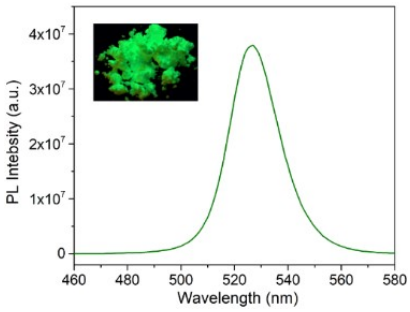

Figure S10 The emission spectrum of Cs_4PbBr_6/FAU-Y composite after exposure to ~45% RH moisture condition for 1 week. Inset: the photograph of Cs_4PbBr_6/FAU-Y samples after exposure for 1 week.

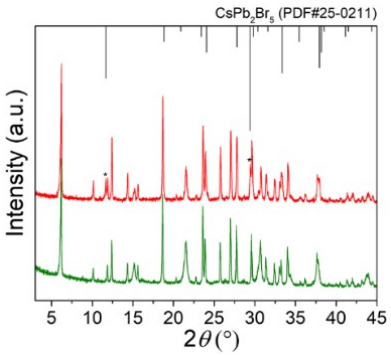

Figure S11 XRD patterns of Cs_4PbBr_6/FAU-Y composite after exposure to air for 2 hours (green) and 1 week (red). The black line pattern is the tetragonal $CsPb_2Br_5$ (PDF #25-0211).

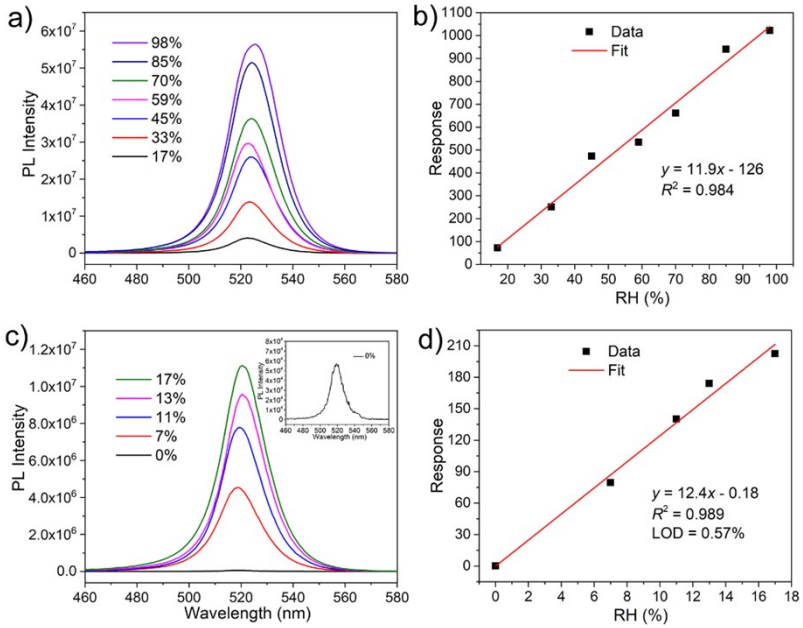

Figure S12 The humidity dependent emission spectra of Cs_4PbBr_6/FAU-Y composite of different synthesis batch after exposure at different RHs for 120 s (a) and 300 s (c). Inset in (c): the emission spectra of Cs_4PbBr_6/FAU-Y at 0% RH. Linear curve between the response and RH of Cs_4PbBr_6/FAU-Y composite after 120 s exposure (b) and 300 s exposure (d).

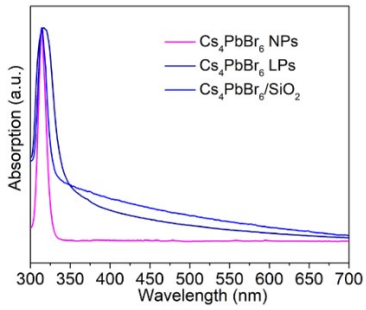

Figure S13 Absorption spectra of Cs_4PbBr_6 NPs, Cs_4PbBr_6 LPs, and Cs_4PbBr_6/SiO_2 in the solution.

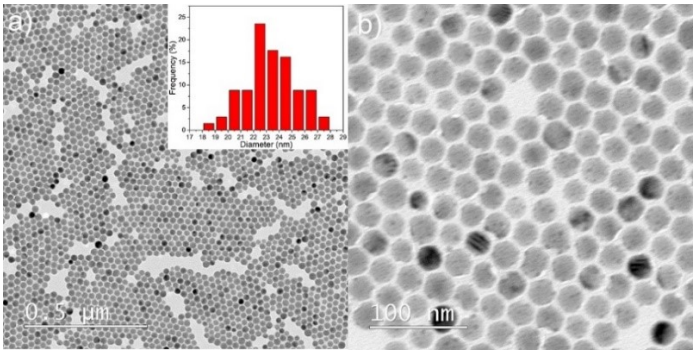

Figure S14 (a) and (b) TEM images of Cs_4PbBr_6 NPs. Inset in (a): the particle size distribution of Cs_4PbBr_6 NPs.

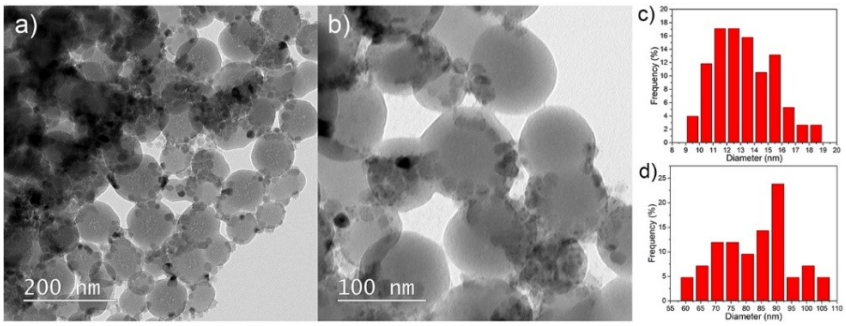

Figure S15 (a) and (b) TEM images of Cs_4PbBr_6/SiO_2. The particle size distributions of Cs_4PbBr_6 (c) and SiO_2 (d).

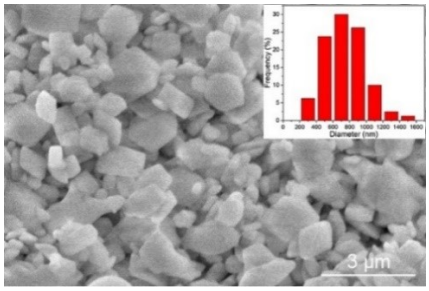

Figure S16 The SEM image of Cs_4PbBr_6 LPs. Inset: the particle size distribution of Cs_4PbBr_6 LPs.

Table S2. The comparison of humidity sensing performances by MHP-based sensors and other fluorescent sensors.

Material	Sensor type	Humidity range (RH)	Response	Sensitivity	LOD (%)	Ref.
Cs_4PbBr_6/FAU-Y	Fluorescence enhancement	7 - 98	1038 ($(I-I_0)/I_0$)	11.8/RH% (17% ≤ RH ≤98%) 12.6/RH% (RH < 17%) ($\Delta Response/\Delta RH$)	0.56%	This work
$CH_3NH_3PbBr_3$	Fluorescence quenching	7 - 98	< 1 ($(I-I_0)/I_0$)	8.50% ($(I_{7\%}-I_{98\%})\times100/I_{98\%}$)	0.68%#	6
EMT-$CsPbBr_3$	Fluorescence enhancement	9 - 92	~18* ($(I-I_0)/I_0$)	~0.19/RH%* ($\Delta Response/\Delta RH$)	0.21%#	7
Cs_4PbBr_6	Fluorescence enhancement	40 - 80	NA	NA	NA	8
$CsPbBr_3$/SAPO-34	Laser quenching	72 - 85	< 1 ($(I-I_0)/I_0$)	24%/RH% ($\Delta I/\Delta RH$)	72%	9
$Cs_2BiAgBr_6$	Resistance change	15 - 78	1162 ($(R_{RH}-R_0)/R_0$)	308 Ω/RH% (25 ℃) ($\Delta R/\Delta RH$)	> 15%	10
$CsPb_2Br_5$-$BaTiO_3$	Capacitance change	25 - 95	NA	21,426 pF/RH% ($\Delta C/\Delta RH$)	> 25%	11
$CsPbBr_3$ nano particles	Resistance change	11 - 95	NA	1.5565%/RH% ($\Delta R/\Delta RH$)	> 11%	12
Cs_2TeCl_6	Resistance change	5 - 90	984 ($(R_{RH}-R_0)/R_0$)	NA	> 5%	13
HA-($Tb_{0.3}Eu_{0.7}$)	Fluorescence quenching	16 - 98	< 1 ($(I-I_0)/I_0$)	0.0261/RH% ($\Delta(I_{Eu}/I_{Tb})/\Delta RH$)	4.3%	14
Poly[1-phenyl-2-(p-trimethylsilyl) phenylacetylene]	Fluorescence quenching	0 - 100	< 1 ($(I-I_0)/I_0$)	NA	20%	15
Zn(II) complex	Fluorescence enhancement	42 - 80	NA	NA	NA	16

TPP	Fluorescent wavelength change	0 - 99	\	0.54 nm/RH% ($\Delta\lambda_{em}/\Delta RH$)	NA	[17]
TVP	Fluorescent wavelength change	0 - 99	\	0.43 nm/RH% ($\Delta\lambda_{em}/\Delta RH$)	NA	[17]
TPE-P/PVP	Fluorescent wavelength change	11 - 95	\	0.57 nm/RH% ($\Delta\lambda_{em}/\Delta RH$)	NA	[18]
TPE-EP/PVP	Fluorescent wavelength change	11 - 95	\	0.65 nm/RH% ($\Delta\lambda_{em}/\Delta RH$)	NA	[18]
DSP@PVP	Fluorescent wavelength change	16 - 95	\	NA	NA	[19]
Zn–BPPA/PEG	Fluorescent wavelength change	18 - 98	\	0.45 nm/RH% (18 - 65%) 3.0 nm/RH% (65 – 88%) ($\Delta\lambda_{em}/\Delta RH$)	NA	[20]
CDs@NaOH	Fluorescent wavelength change	6.9 – 95.4	\	NA	NA	[21]

NA: Not Applicable; *: We calculated the sensitivity value based on data from the corresponding article to compare with the other sensors; #: the LOD value was calculated by a different method in the corresponding article, which used the slope of the linearity between PL intensity and RH.

Notes and references

1. L. Wu, H. Hu, Y. Xu, S. Jiang, M. Chen, Q. Zhong, D. Yang, Q. Liu, Y. Zhao, B. Sun, Q. Zhang and Y. Yin, *Nano Lett.*, 2017, **17**, 5799-5804.
2. L. Yang, D. Li, C. Wang, W. Yao, H. Wang and K. Huang, *J. Nano Res.*, 2017, **19**, 1-13.
3. J. Rodríguez-Carvajal, *Phys. Rev., B Condens. Matter*, 1993, **192**, 55-69.
4. P. W. Winston and D. H. Bates, *Ecology*, 1960, **41**, 232-237.
5. O. A. Ponomareva, P. A. Shaposhnik, M. V. Belova, B. A. Kolozhvari and I. I. Ivanova, *Front. Chem. Sci. Eng.*, 2018, **12**, 70-76.
6. W. Xu, F. Li, Z. Cai, Y. Wang, F. Luo and X. Chen, *J. Mater. Chem. C*, 2016, **4**, 9651-9655.
7. X. Zhang, J. Lv, J. Liu, S. Xu, J. Sun, L. Wang, L. Xu, S. Mintova, H. Song and B. Dong, *J. Colloid Interf. Sci.*, 2022, **616**, 921-928.
8. X. Y. Yu, L. Z. Wu, H. C. Hu, M. Chen, Y. S. Tan, D. Yang, Q. Pan, Q. X. Zhong, T. Supasai and Q. Zhang, *Langmuir*, 2018, **34**, 10363-10370.
9. R. Li, J. Yu, S. Wang, Y. Shi, Z. Wang, K. Wang, Z. Ni, X. Yang, Z. Wei and R. Chen, *Nanoscale*, 2020, **12**, 13360-13367.
10. Z. Weng, J. Qin, A. A. Umar, J. Wang, X. Zhang, H. Wang, X. Cui, X. Li, L. Zheng and Y. Zhan, *Adv. Funct. Mater.*, 2019, **29**, 1902234.

11. M. Y. Cho, S. Kim, I. S. Kim, E. S. Kim, Z. J. Wang, N. Y. Kim, S. W. Kim and J. M. Oh, *Adv. Funct. Mater.*, 2020, **30**, 1907449.
12. Z. Wu, J. Yang, X. Sun, Y. Wu, L. Wang, G. Meng, D. Kuang, X. Guo, W. Qu and B. Du, *Sens. Actuators B Chem.*, 2021, **337**, 129772.
13. C. Pi, X. Yu, W. Chen, L. Yang, C. Wang, Z. Liu, Y. Wang, J. Qiu, B. Liu and X. Xu, *Mater. Adv.*, 2021, **2**, 1043-1049.
14. D. Xia, J. Li, W. Li, L. Jiang and G. Li, *J. Lumin.*, 2021, **231**, 117784.
15. M. Trigo-López, A. Muñoz, S. Ibeas, F. C. García, F. Serna and J. M. García, *Sens. Actuators B Chem.*, 2014, **191**, 233-238.
16. A. Wang, R. Fan, Y. Dong, Y. Song, Y. Zhou, J. Zheng, X. Du, K. Xing and Y. Yang, *ACS Appl. Mater. Interfaces* 2017, **9**, 15744-15757.
17. Y. Cheng, J. Wang, Z. Qiu, X. Zheng, N. L. Leung, J. W. Lam and B. Z. Tang, *Adv. Mater.*, 2017, **29**, 1703900.
18. Y. Jiang, Y. Cheng, S. Liu, H. Zhang, X. Zheng, M. Chen, M. Khorloo, H. Xiang, B. Z. Tang and M. Zhu, *Natl. Sci. Rev.*, 2021, **8**, 135.
19. R. Gao, D. Cao, Y. Guan and D. Yan, *Ind. Eng. Chem. Res.*, 2016, **55**, 125-132.
20. J. Wei, Y. Ma, C. Liu, J. Li, J. Shen, K. Y. Zhang, S. Liu and Q. Zhao, *J. Mater. Chem. C*, 2021, **9**, 5945-5951.
21. Z. Z. Ding, G. S. Zheng, Q. Lou, J. F. Han, M. Y. Wu, C. L. Shen, J. H. Zang, K. K. Liu, L. Dong and C. X. Shan, *J. Phys. D Appl. Phys.*, 2022, **55**, 154001.